Colloid Polym Sci (2007) 285:1593–1600
DOI 10.1007/s00396-007-1730-9

ORIGINAL CONTRIBUTION

Controllable synthesis of ZnS/PMMA nanocomposite hybrids generated from functionalized ZnS quantum dots nanocrystals

Lei Guo · Su Chen · Li Chen

Received: 31 May 2007 / Revised: 21 June 2007 / Accepted: 22 June 2007 / Published online: 28 July 2007

Abstract We reported controllable synthesis of ZnS nanocrystal-polymer transparent hybrids by using polymethylmethacrylate (PMMA) as a polymer matrix. In a typical run, the appropriate amounts of zinc chloride ($ZnCl_2$) and sodium sulfide (Na_2S) in the presence of 2-mercaptoethanol (ME) as the organic ligand were well dispersed in H_2O/dimethylformamide solution without any aggregation. In addition, the Mn-doped ZnS nanocrystals (NCs) were synthesized with similar method. Then, ZnS-PMMA hybrids were obtained via free radical polymerization in situ by using ZnS NCs functionalized with methacryloxypropyltrimethoxysilane (MPS). FT-IR characterization indicates the formation of robust bonding between ZnS NCs and the organic ligand. The TEM images show that ZnS NCs are well dispersed in PMMA matrix, and particle size of as-prepared ZnS NCs is about 2.6 nm, in agreement with the computing results of Brus's model and Debye–Scherrer formula. The photoluminescence measurements present that ZnS NCs, Mn-doped ZnS NCs, and ZnS/PMMA hybrid show good optical properties.

Keywords ZnS NCs · Polymethylmethacrylate · Hybrids · Optical properties · Quantum dots

Introduction

Semiconductor nanocrystals (NCs) have received much recent interest for their unusual optical and electronic properties [1], such as the potential in lasers [2, 3], biological labeling [4–6], light-emitting diodes (LEDs) [7, 8], and devices [9, 10]. Because of their unique and size-dependent properties arising from quantum confinement and surface effect, ZnS NCs have been extensively studied [11–16]. In particular, ZnS NCs are often employed to be new luminescence center via doping different ions due to its large band-gap energy [17–20]. By now, a large number of techniques for preparing ZnS NCs, such as sol–gel [21, 22], template [23, 24], vapor deposition [25], micelles [26], and solvent growth [27–29], have been applied. Among them, the solvent growth technique is very effective in yielding a narrow size distribution and optimization of the properties in preparation of NCs. To this end, a variety of efforts have been carried out via arrested precipitation to synthesize quantum dots (QDs) ZnS NCs, including simple inorganic ions by aid of cysteine [27] stabilizer or low molecular weight thiols stabilizers [30, 31], and zinc ethylxanthate in trioctyl phosphine by aid of hexadecylamine as a stabilizer [32].

The organic–inorganic polymer nanocomposites combining both the properties of inorganic and organic materials offer unique mechanical, thermal, and optical features and can apply in versatile areas. There are many methods for attaching polymer chains onto nanoparticle surfaces, including in situ synthesis of nanocomposites [33–35], chemisorption, [36] covalent attachment of end-functionalized polymers to a reactive surface ("grafting to") [37–40], and in situ monomer polymerization with monomer growth of polymer chains from immobilized initiators (grafting from) [41–44]. To allow ZnS NCs to embed in polymer matrix, many research groups have reported on the preparation and applications of ZnS/polymer nanocomposites [45–50]. Recently, polymer light-emitting materials were synthesized by ZnS nanoparticles hybridized with poly(acrylic acid) [45]. Bai et al. [46] reported synthesis of

L. Guo · S. Chen (✉) · L. Chen
State Key Laboratory of Material-Oriented Chemical Engineering,
Nanjing University of Technology,
No. 5 Xin Mofan Rd.,
Nanjing 210009, People's Republic of China
e-mail: prcscn@yahoo.com.cn

composite microspheres containing patterned structure ZnS NCs by using poly(*N*-isopropylacrylamide-co-methacrylic acid) microgels as templates. Pich et al. [47] explored the preparation of ZnS nanocomposites with the method of ultrasonication. Lu et al. [48] prepared ZnS NCs/polythiourethane via ultraviolet radiation-initiated free radical polymerization. ZnS/poly(acrylamide-co-acrylic acid) dendritical nanocomposites were prepared through γ-irradiation [49]. In a recent letter, we fabricated NC-polyurethane hybrids successfully [50].

In this work, we present a simple procedure for fabrication of functionalized ZnS NCs and ZnS/polymethylmethacrylates (PMMA) nanocomposite hybrids via graft copolymerization. The hydroxyl-capped ZnS NCs were prepared through the reaction between zinc chloride and sodium sulfide in the presence of 2-mercaptoethanol (ME) as the organic ligands. In addition, Mn-doped ZnS NCs were synthesized with the similar method. Although a number of investigations on ZnS NCs have been reported in literatures [51, 52], there are few reports presenting the photographs of ZnS NCs taken under ultraviolet light to prove their good photoluminescence (PL) properties. In this case, we present the photographs of ZnS NCs and Mn-doped ZnS NCs taken under ultraviolet light to directly indicate their optical properties. The key point for preparing high-performance NC-polymer hybrids is how to produce good PL materials, along with excellent transparency. Considering NCs have high surface area and surface energy, and are easy to aggregate in the polymer matrix, we employ methacryloxypropyltrimethoxysilane (MPS) to prepare functionalized ZnS NCs containing double bonds. Therefore, dangling double bonds to some extent remain on the surface of functionalized ZnS NCs, allowing them to further graft into PMMA matrix in situ. Finally, controllable synthesis of well-defined transparent ZnS NC-PMMA nanocomposite hybrids has been successfully carried out. FT-IR was used to characterize the chemical structure for the functionalization of ZnS NCs. In addition, the properties of ZnS/PMMA nanocomposite hybrids were throughout investigated by TGA, TEM, AFM, ultraviolet-visible (UV-vis) absorption, and PL spectra.

Experimental

Materials ME, zinc chloride ($ZnCl_2$), manganese chloride ($MnCl_2$), sodium sulfide ($Na_2S{\cdot}9H_2O$), methyl methacrylates (MMA), 2, 2-azobis isobutyronitrile (AIBN), and *N*, *N*-dimethylformamide (DMF) were supplied by Aldrich and used as received. DMF was dried over 4 Å molecular sieves and used without further purification. MPS was supplied by Nanjing Crompton Shuguang Chemical Organosilicon Specialties.

Synthesis of hydroxyl-coated ZnS NCs In the first step, 5 mmol of zinc chloride in 40 ml of DMF was continuously stirred and mixed with 10 mmol of ME in 4 ml of deionized water. In the second step, 4 ml of aqueous solution of sodium sulfide (Na_2S: 3 mmol) was slowly added dropwise into the above solution under stirring. Once added, the color of the above solution turned white immediately. Then, the reaction was carried out for additional 6 h at room temperature. Finally, the white solution gradually turned to be transparent. The amount of water and salts in the transparent ZnS NC suspension thus obtained were removed, respectively, and then washed by fresh DMF solvent for several times.

Synthesis of hydroxyl-coated manganese-doped ZnS NCs (ZnS:Mn) In a typical procedure, 5 mmol of zinc chloride in 56 ml of DMF was continuously stirred and mixed with 3.2 ml of aqueous solution of manganese chloride ($MnCl_2$: 2 mmol). In the second step, 4 ml of aqueous solution of ME (10 mmol) was slowly added dropwise into the above solution under stirring. Then, sodium sulfide (Na_2S: 3 mmol), which was dissolved in 4 ml deionized water, was added dropwise into the resulting complex (the molar ratio between the total amount of salt and sulfur is controlled to be 10:6). Once added, the color of the above solution turned white immediately. The reaction was carried out for additional 6 h at room temperature. Finally, the white solution gradually turned to be transparent.

Functionalizing of ZnS NCs with MPS The hydroxyl-coated ZnS NC suspensions (in DMF) obtained from the above step was diluted with stoichiometric fresh DMF. The mixture of given amount of ZnS NC suspensions diluted with DMF and MPS (ZnS NC: MPS=1: 0.75 wt/wt) was stirred vigorously under nitrogen at 110 °C for 12 h. Finally, the MPS tethered ZnS NCs, which contain double bonds to further polymerize with MMA monomers, were done.

Synthesis of ZnS NC-PMMA nanocomposite hybrids The ZnS NC-PMMA nanocomposite hybrid was synthesized via free radical polymerization in situ by one step, with AIBN, ZnS NCs, MMA (AIBN: ZnS NCs: MMA=0.003: 0.06: 1 wt/wt/wt, MMA accounts for 10 wt% of the total weight), the appropriate amounts of MPS functionalized ZnS NC suspensions (in DMF), 2,2-azobis isobutyronitrile (AIBN; as the initiator) and stoichiometric fresh DMF (as the solvent) carried out in a three-necked glass reactor equipped with a stirrer, a reflux condenser, and thermocouples and was stirred under nitrogen at 70 °C. Subsequently, a solution of MMA was then added dropwise for half an hour. To produce ZnS NC-PMMA nanocomposite hybrids, the mixture was stirred vigorously under nitrogen

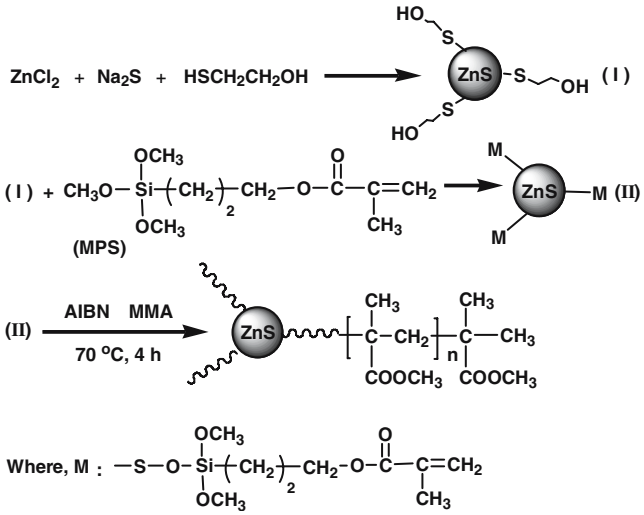

Scheme 1 Synthesis of hydroxyl-coated ZnS NCs and ZnS/PMMA nanocomposite hybrids

at 70 °C for another 4.5 h. The schematic synthesis of hydroxyl-coated functional ZnS NC, double-bond functionalized ZnS NC, and ZnS/PMMA nanocomposite hybrids is shown in Scheme 1.

Characterization UV-vis absorption spectra were taken with a Perkin–Elmer Lambda 900 UV-vis spectrometer with the scan rang from 260 to 450 nm using DMF as solvent. The powder X-ray diffraction (XRD) patterns were conducted on a Bruker-AXS D8 ADVANCE X-ray diffractometer at a scanning rate of 6°/min in 2θ ranging from 10° to 80° with CuKα radiation (λ=0.1542 nm). Fourier transform infrared (FT-IR) spectra were recorded on a NICOLET-NEXUS 670 spectrometer. The samples were grounded with KBr crystal and the mixture of them was pressed into a flake for IR measurement. A high-resolution transmission electron microscope (HRTEM; Model JEOL JEM-2100 electron microscope) was conducted on JEOL JEM-2010 TEM at an acceleration of 200 kV and used to observe the morphology of the NC and the nanocomposites. The samples were dispersed in DMF, and a drop of the solution was placed on a copper grid that was left to dry before transferring into the TEM sample chamber. Atomic force microscopy (AFM) measurement was performed by a PSI AutoCP-Research AFM using tapping mode in air. PL spectra were measured on a VARIAN Cary Eclipse fluorescence spectrophotometer operating with a 300-nm laser beam as a light source and with Xe-lamp as the excited source, the tube voltage was 600 V, and the excitation and emission slits were both 5 nm. All the PL samples were diluted 60 times with DMF for analysis and performed under ambient conditions. The weight-loss of the ZnS/PMMA hybrids on heating was studied by TGA using a thermogravimetric apparatus Shimadzu-TGA 50 under a nitrogen atmosphere. Measurements were taken with a heating rate of 10 °C/min from 50 to 600 °C. The sample was prepared by drying in a vacuum oven at 90 °C for 2 days at a pressure of 70 kPa for solvent removal.

Results and discussion

Our preliminary work focuses on how to prepare quantum dots ZnS NCs. The synthesis of hydroxyl functionalized ZnS NCs involves the reaction between zinc and sulfur ions in the presence of ME as the organic ligands. The electron-deficient atoms of zinc on the surface of semiconductor serve as binding sites to anchor organic ligands, and to hinder the further growth of crystal grains, leading the formation of nanosized crystals.

To investigate the quantum effect of the NCs, we measured UV-vis spectrum of ZnS NCs and estimated the particle size of ZnS NCs through UV-vis and XRD characterization. Figure 1 shows the UV-vis absorption spectrum of the ZnS NCs. An intense peak is noticed at 272 nm (4.56 eV), while absorption characteristic peak of ZnS bulk material appears at 340 nm (3.66 eV). Thus, blue shift of absorption in UV-vis spectrum of ZnS NCs occurs due to their quantum effect. According to Brus' model, the exited energy of NCs is reverse to their particle size. The particle size of ZnS NCs can be calculated by the position of the maximum absorption in UV-vis spectra according to the following Brus formula [53–55]. For ZnS NCs, assuming the effective mass of electron m_e=0.40 and hole mass m_h=0.61 with dielectric constant ε=5.2 [30], the

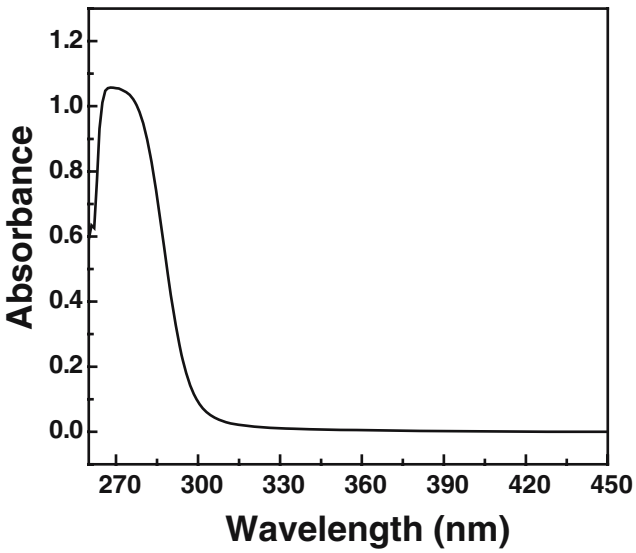

Fig. 1 UV-vis absorption spectrum of the ZnS NCs prepared by molar ratio of ME/Zn^{2+}/S^{2-}=2/1/0.6 mol/mol; solvent: H_2O/DMF= 2/10 wt/wt; reaction time: 6 h

radius of the NCs was calculated to be 1.31 nm, which means particle diameter of ZnS NC is 2.62 nm. In addition, the effect of quantum confinement is observable.

$$E^* = E_g + \frac{h^2}{8R^2}\left[\frac{1}{m_e} + \frac{1}{m_h}\right] - 1.8\frac{e^2}{\varepsilon R}$$

To obtain more structure information of ZnS NCs, we measure XRD of ZnS NCs (shown in Fig. 2). As seen in Fig. 2, the three diffraction features appearing at about 28.8, 47.9, and 56.3° correspond to the (111), (220), and (311) planes of the zinc blende phase of ZnS, respectively. In addition, the particle size was calculated according to the following Debye–Scherrer formula [31].

$$L = \frac{0.9\lambda}{B\cos\theta}$$

Where L is the coherence length, B is the full width at half maximum (FWHM) of the diffraction peak, λ is the wavelength of the X-ray radiation, and θ is the Bragg angle of the diffraction peak. The relation between L and D, the diameter of the crystallite, is given by L=3/4D, assuming the particles are spherical in shape. The value of L obtained for ZnS NCs is 1.909 nm, which means the particle diameter of ZnS NCs is 2.54 nm, in good agreement with the result obtained from the UV-vis absorption spectrum. These results indicate that as-prepared ZnS NCs show quantum dots.

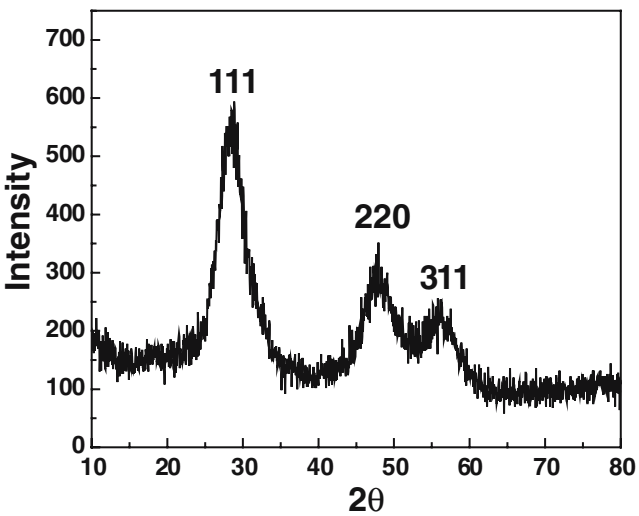

Fig. 2 The powder X-ray diffraction pattern of ZnS NCs prepared by molar ratio of ME/Zn^{2+}/S^{2-}=2/1/0.6 mol/mol; solvent: H_2O/DMF=2/10 wt/wt; reaction time: 6 h

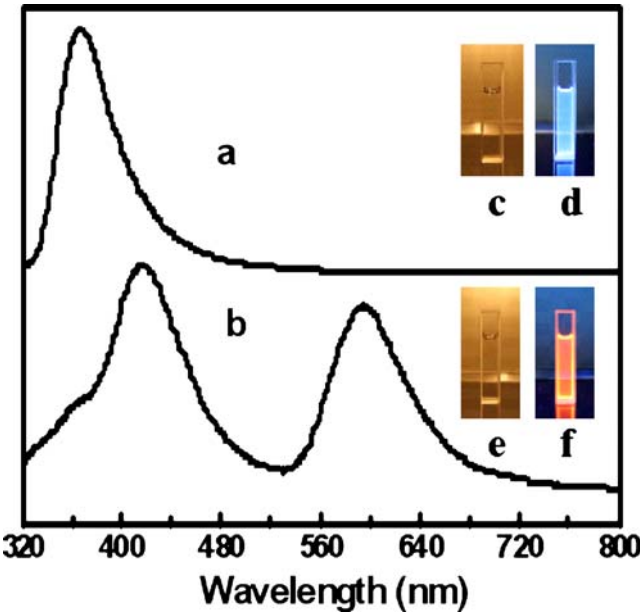

Fig. 3 The photoluminescence emission spectra for **a** undoped ZnS NCs prepared by molar ratio of ME/Zn^{2+}/S^{2-}=2/1/0.6 mol/mol; solvent: H_2O/DMF=2/10 wt/wt; reaction time: 6 h, and **b** Mn-doped ZnS NCs prepared by molar ratio of ME/(Zn^{2+}+Mn^{2+})/S^{2-}=2/1/0.6 (mol/mol); Zn^{2+}/Mn^{2+}=10/4 (mol/mol); solvent: H_2O/DMF=2/10; excitated at 300 nm. The photographs of ZnS NCs and Mn-doped ZnS NCs suspension in DMF (**c**, **e**) under a daylight lamp and (**d**, **f**) under 302-nm ultraviolet light

As a typical semiconductor, ZnS NCs show interesting optical properties. Especially, ZnS NCs doped with optically active PL center create new opportunities in PL study and application of nanoscale materials. Figure 3 shows the PL emission spectra for the (a) undoped and (b) Mn-doped ZnS NCs recorded at an excitation wavelength of 300 nm. In the undoped ZnS NCs, we observe only one single emission at 360 nm, which exhibits a well-defined excitonic emission feature. This emission behavior is consistent with a recent report on highly luminescent ZnS NCs [56]. In Fig. 3b, the characteristic emissions for Mn-doped ZnS NCs are about 415 and 590 nm, respectively. The peak appearing in 415 nm corresponds to the defect-state emission of Mn-doped ZnS NCs [57]. In addition, with Mn-doped in the NC samples, new emission develops at 590 nm is attributed to the well-known $^4T_1$–$^6A_1$ Mn transition. Figure 3c and e are the photographs of the ZnS NC and Mn-doped ZnS NC taken under daylight, respectively. As seen in Fig. 3c and e, they all present colorless and transparent under the daylight. Figure 3d and f are the photographs of the ZnS NC and Mn-doped ZnS NC taken under 302-nm ultraviolet light, respectively. The ZnS NCs suspension displays light blue color under 302-nm ultraviolet light, corresponding to the normalized PL spectra with maximum wavelength at 360 nm. Whereas Mn-doped ZnS NC suspension displays orange color under 302-nm ultraviolet light, corresponding to the normalized PL

spectra with maximum wavelength at 590 nm. According to the report of Bhargava et al. [58], the luminescent efficiency of the NCs increases with decreasing particle size of NCs, meaning smaller particle size of NCs exhibits good luminescent properties. That is why ZnS NCs and Mn-doped ZnS NCs quantum dots exhibit the good luminescence property.

To embed NCs into PMMA matrix, we first prepared ZnS NCs using ME as organic ligand. Then, the resultant ZnS NCs were further modified with MPS, allowing methacrylate groups to attach onto the surface of NCs. Finally, the functionalized ZnS NCs could be successfully incorporated into PMMA matrix via free radical polymerization. The schematic synthesis of hydroxyl-coated functional ZnS NC, double-bond functionalized ZnS NC, and ZnS/PMMA nanocomposite hybrids is shown in Scheme 1.

To get better understanding of the assembly of ZnS NCs and organic polymer, we employed FT-IR to characterize ZnS NCs and functionalized ZnS NCs, respectively. For the FT-IR spectrum of ZnS NCs, strong absorption peaks at 1,060 and 1,000 cm^{-1} (νC–O) show that abundant hydroxyl groups are tethered on the surface of ZnS NCs. The absorption peaks at 2,920 cm^{-1}, 2,850 cm^{-1} (νC–H), and 1420 cm^{-1} (νCH_2) indicate the existence of the methylene group. In this case, there are no any characteristic peaks of the mercapto group in FT-IR spectrum, which the wavenumber of absorption peak ranges from 2,500 to 2,600 cm^{-1}, indicating that the free mercapto groups almost disappeared and the robust bonding between Zn^{2+} and ME organic ligand formed. The hydroxyl group thus introduced onto the surface of NCs not only allows the NCs to be dispersed well in solvent but also provides the possibility for further assembling with organic polymers. For the FT-IR spectrum of MPS functionalized ZnS NC, the FT-IR results indicate that the characteristic absorption peaks of carbonyl group (1,740 cm^{-1}), C–O–C group (1,160 cm^{-1}), and Si–O–C group (1,050 cm^{-1}) may indicate that the hydroxyl of the ligand on the surface NCs has reacted with methoxy group of MPS via condensation reaction, which can prove that the double-bond group in the functionalized ZnS NCs exists after condensation reaction. On the other hand, the MPS tethered ZnS NCs may allow themselves to be very compatible in PMMA matrix. The doped NCs are virtually considered as cross-linking dots during the assembly of NCs and PMMA. In addition, the tethered polymer chains further restrain the aggregation among the NCs.

Figure 4 demonstrates the typical TEM images of the as-prepared ZnS/PMMA nanocomposite hybrid. In Fig. 4a, it is found that the ZnS NCs are well dispersed in the polymer matrix without any aggregation. High-resolution TEM picture shown in Fig. 4b indicates the presence of microstructure in the coarsened ZnS NCs. The observed particle size of ZnS NC is nearly 2.6 nm, which is in agreement with the results calculated by the Brus's model and Debye–Scherrer formula. On the other hand, the existence of lattice planes on the magnified ZnS NC further confirm the crystallinity of ZnS nanoparticles. Detailed analysis on the lattice fringes gives an interplanar spacing of 0.31 nm, which is in agreement of the recently reported cubic structure ZnS [59]. The above results also present that as-prepared ZnS NCs still show quantum dots in the PMMA matrix. The dispersibility of ZnS NCs in polymeric matrices can be enhanced when the PMMA chains graft onto ZnS nanoparticles.

The AFM was used to characterize the morphology of polymer hybrid film. The ZnS/PMMA nanocomposite film was prepared with the spin coater and the surface morphology of the resulting film was determined by AFM in contact mode. AFM image from the top surface of the sample reveals the mound patterns as shown in Fig. 5a. It is also found that lots of homogeneous mounds (white part)

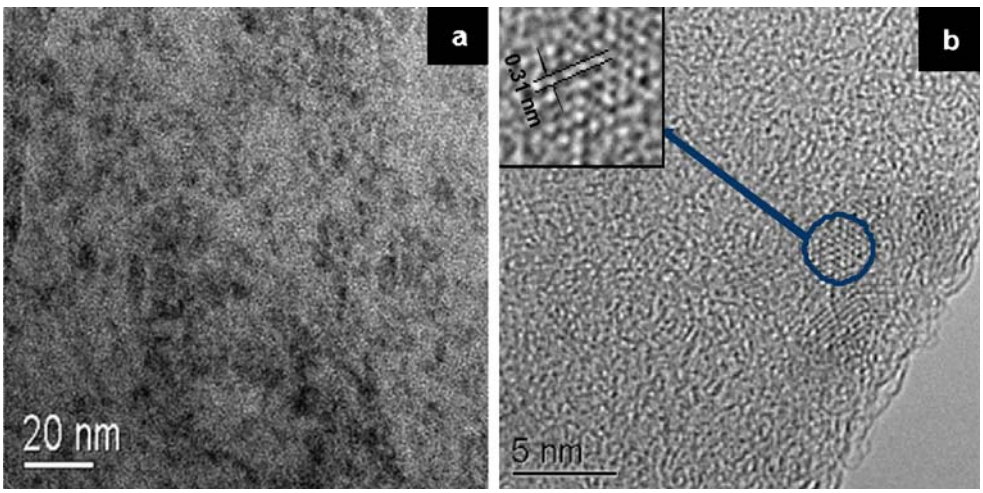

Fig. 4 **a** Low-magnification TEM picture of ZnS/PMMA nanocomposite hybrid. **b** High-resolution TEM picture of ZnS/PMMA nanocomposite hybrid. ZnS/MMA=6/100 wt/wt, AIBN/MMA=0.3 wt%, MMA wt%=10 wt%, reaction time: 4.5 h

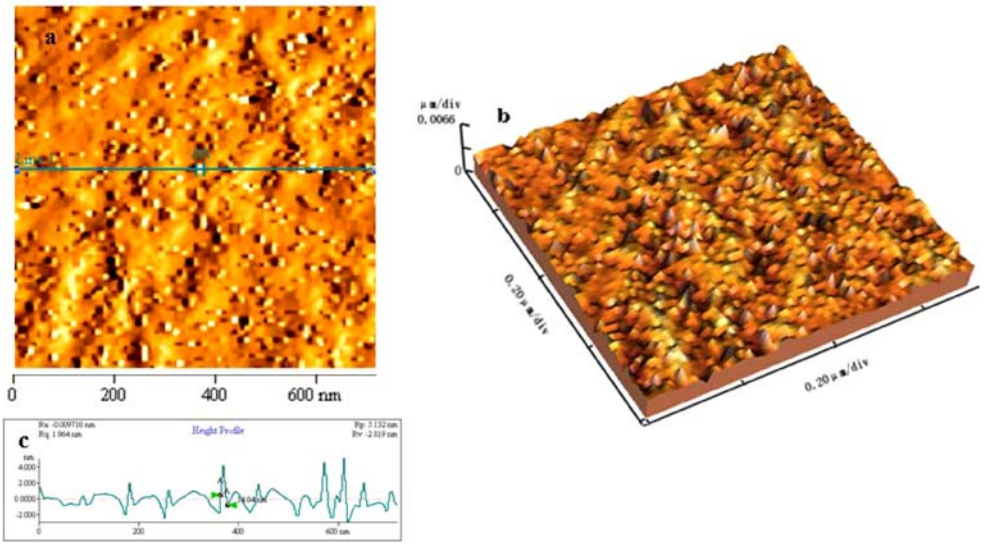

Fig. 5 **a** AFM image of a surface of spin-cast film for ZnS/PMMA nanocomposite. **b** Three-dimensional AFM image of the surface of the film for ZnS/PMMA nanocomposite. ZnS/MMA=1/100 wt/wt, AIBN/MMA=0.3 wt%, MMA=10 wt%, reaction time: 4.5 h, the rotation speed for spin casting was 1,500 rpm. **c** The height profile of the AFM image for the ZnS/PMMA nanocomposite film

are well-dispersed in three-dimensional representation of the film as showed in Fig. 5b. The height profile of the AFM image for the ZnS/PMMA nanocomposite film is presented in Fig. 5c. The mounds of the film have a height of 2–5 nm and a diameter of 10–20 nm as estimated from AFM image. AFM results also present that the particle size of the ZnS NCs is larger than those observed from TEM image. It may be explained that ZnS NCs are surrounded by PMMA chains, and the hybrid topographical microspheres with larger size may be formed. On the other hand, the mean square roughness of ZnS/PMMA nanocomposite film is quite low (Rq=1.064), although a large number of mounds are observed in the surface of the film, which confirms the excellent planarity of the surface. Low roughness reduces the scattering loss at the surface, and good optical property is expected to be obtained on the surface of ZnS/PMMA nanocomposite film.

To investigate on optical properties of ZnS/PMMA hybrids, we employed UV-vis absorption and PL spectra to characterize ZnS/PMMA hybrids, along with characterizing the pure PMMA for comparison.

Figure 6 is UV-vis absorption spectra of pure PMMA and ZnS/PMMA hybrid with different concentrations of ZnS NCs. As seen in Fig. 6, the absorption peak of pure PMMA appears at a wavelength of 265 nm, while the absorption peaks of PMMA nanocomposites are broadened in the range from 265 to 285 nm. In addition, UV-vis absorption spectra of the as-prepared nanocomposite hybrids display an obvious red shift, which are compared with pure PMMA. In addition, the strength of absorption peaks of PMMA nanocomposites are enhanced with the increase in ZnS NCs concentration. The result also indicates that ZnS NCs show quantum dots in the ZnS/PMMA nanocomposite hybrid.

As a typical semiconductor, ZnS NCs exhibit interesting optical properties. With the ZnS NCs embedded in the PMMA matrix, the ZnS/PMMA hybrids show excellent optical characteristic property. Figure 7 is the PL emission spectra of pure PMMA and ZnS/PMMA nanocomposite hybrid with excitation at 300 nm. As seen in Fig. 7a, there is no obvious PL in pure PMMA, whereas a strong absorption peak at 360 nm can be observed in ZnS NCs suspension in Fig. 7b, which exhibits a well-defined excitonic emission feature [53, 56]. Figure 7c shows that

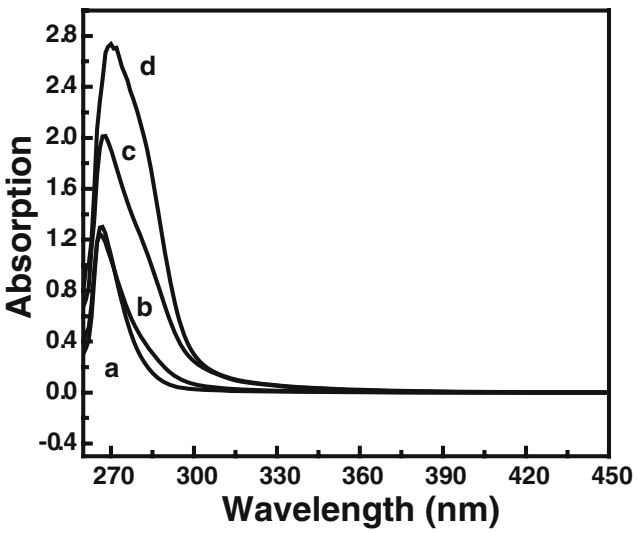

Fig. 6 UV-vis absorption spectra of ZnS/PMMA hybrids diluted with DMF (**a** pure PMMA, AIBN/PMMA=0.3 wt%, MMA wt %=10 wt%, reaction time: 4.5 h, dispersed in DMF; **b** ZnS/PMMA hybrid, ZnS/MMA=1/100 wt/wt, AIBN/MMA=0.3 wt%, MMA=10 wt%, reaction time: 4.5 h, dispersed in DMF; **c** ZnS/PMMA hybrid, ZnS/MMA=3/100 wt/wt, AIBN/MMA=0.3 wt%, MMA wt%=10 wt%, reaction time: 4.5 h, dispersed in DMF; **d** ZnS/PMMA hybrid, ZnS/MMA=6/100 wt/wt, AIBN/MMA=0.3 wt%, MMA wt%=10 wt%, reaction time: 4.5 h, dispersed in DMF)

an increase in the emission peak strength occurs in ZnS/PMMA hybrid solution. It may be explained that an effect of environment broadening allows the surface structure of ZnS NCs to be changed when ZnS NCs embedded in PMMA matrix, resulting into ZnS/PMMA hybrid, exhibit good optical property.

To understand the thermal stability of ZnS NCs embedded in PMMA matrix, we used TGA measurement to characterize the ZnS/PMMA hybrid, along with characterizing pure PMMA polymer for comparison. Figure 8 is the represented TGA diagrams of the ZnS/PMMA hybrid and pure PMMA polymer. There is a single degradation step in the curve, owing to the decomposition of PMMA polymer matrix. For pure PMMA polymer, the decomposition of PMMA polymer occurs at 250–420 °C, while in Fig. 8b the decomposition of about 85% PMMA nanocomposite occurs at 300–460 °C. This clearly shows that the nanocomposite exhibits considerably enhancement in the thermal stability. The interaction between the NCs and the polymers are so firm that the thermal degradation of the polymers become more difficult [60].

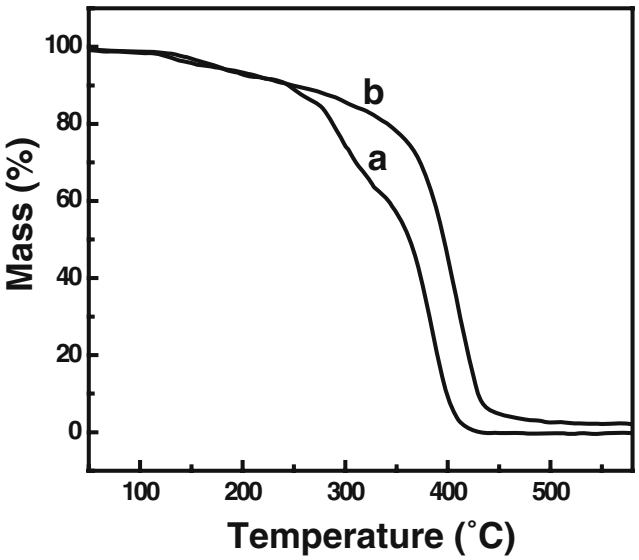

Fig. 8 TGA plots of **a** pure PMMA polymer, AIBN/MMA=0.3 wt%, MMA=10 wt%, reaction time: 4.5 h; and **b** ZnS/PMMA nanocomposite, ZnS/MMA=1/100 wt/wt, AIBN/MMA=0.3 wt%, MMA=10 wt%, reaction time: 4.5 h

Conclusions

The first facile controllable synthesis of ZnS/PMMA nanocomposites has been achieved. First, ZnS NCs are obtained by the reaction between zinc chloride ($ZnCl_2$) and sodium sulfide (Na_2S) in the presence of ME as the organic ligand. Furthermore, Mn-doped ZnS NCs with good luminescence property could be synthesized with the similar method. Then, the hydroxyl-ending alkyl group thus introduced onto the surface of ZnS NCs enhances their dispersity in solvent, allowing the particle size of NCs to be controlled. We have found that the particle size of the ZnS NC characterized by TEM is about 2.6 nm, in agreement with the calculated data from UV-vis absorption spectra according to Brus's model and Debye–Scherrer formula.

Second, we used MPS to further functionalize ZnS NCs and allow them to contain double bonds. Therefore, we successfully fabricated ZnS/PMMA nanocomposite hybrids via free radical polymerization in situ. FT-IR characterization indicates the formation of robust bonding between ZnS NCs and the organic ligand and the formation of double-bond functional ZnS NCs. The TEM images indicate that ZnS NCs are well dispersed in PMMA matrix. AFM characterization shows the transparent ZnS/PMMA hybrid film show mound patterns with lateral sizes ranging from 10 to 20 nm. The TGA measurement displays ZnS-PMMA hybrids possess better thermal stability than those of pure PMMA polymer. The fluorescence measurement indicates that ZnS/PMMA hybrids also exhibit good optical properties.

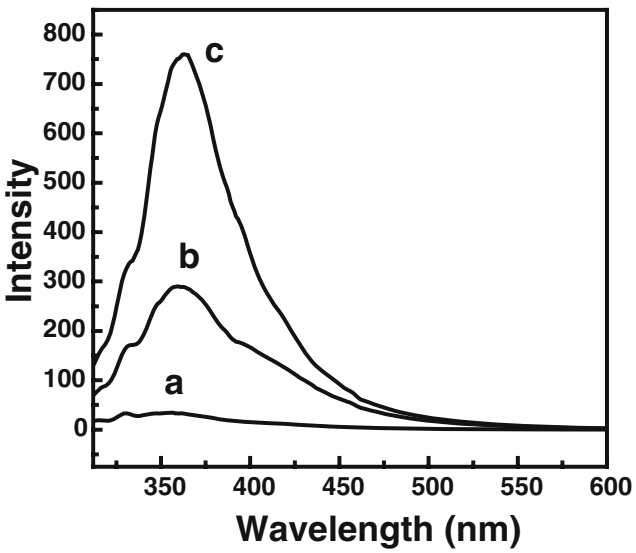

Fig. 7 Photoluminescence spectra of pure PMMA and ZnS/PMMA nanocomposite hybrids diluted with DMF excitated at 300 nm. (**a** pure PMMA, AIBN/PMMA=0.3 wt %, MMA wt%=10 wt%, reaction time: 4.5 h, dispersed in DMF; **b** hydroxyl-coated ZnS NCs suspension; **c** ZnS/PMMA hybrid, ZnS/MMA=6/100 wt/wt, AIBN/MMA=0.3 wt%, MMA wt%=10 wt%, reaction time: 4.5 h, dispersed in DMF)

Acknowledgments This work was supported by the National Natural Science Foundation of China (grant no. 20576053, 10676013, 20606016), the Natural Science Foundation of Jiangsu province, China (grant no. BK2005119), and the Natural Science Foundation of the Jiangsu Higher Education Institutions of China (grant no. 04KJB430038).

References

1. Alivisatos AP (1996) J Phys Chem 100:13226
2. Artemyev MV, Woggon U, Wannemacher R, Jaschinski H, Langbein W (2001) Nano Lett 1:309
3. Ghosh S, Mukherjee A, Lee C (2003) Mater Chem Phys 78:726
4. Jaiswal JK, Mattoussi H, Simon SM (2003) Nat Biotechnol 21:47
5. Chan WCW, Nie SM (1998) Science 281:2016
6. Lidke DS (2004) Physiology 19:322
7. Coe S, Woo WK, Bulovic V (2002) Nature 420:800
8. Tesster N, Medvedev V, Banin U (2002) Science 295:1506
9. Zhu L, Zhu MQ, Hurst JK, Li AD (2005) J Am Chem Soc 127:8968
10. Kho R, Mehra RK (2000) J Colloid Interface Sci 227:561
11. Khitrov GA, Strouse GF (2003) J Am Chem Soc 125:10465
12. Li Y, Li X, Yang C (2004) J Phys Chem B 108:16002
13. Lu HY, Chu SY (2004) J Cryst Growth 265:476
14. Pich A, Hain J, Lu Y (2005) Macromolecules 38:6610
15. Zhong XH, Liu SH, Zhang ZH, Li L, Wei Z, Knoll W (2004) J Mater Chem 14:2790
16. Chen W, Joly AG, Malm JO, Bovin JO, Wang S (2003) J Phys Chem B 107:6544
17. Sapra S, Prakash A, Ghangrekar A, Periasamy N, Sarma DD (2005) J Phys Chem B 109:1663
18. Malik MA, Revaprasadu NJ (2001) Mater Chem 11:2382
19. Karar N, Raj S, Singh F (2004) J Cryst Growth 268:585
20. Zhang Y, Li Y (2004) J Phys Chem B 108:17805
21. Donahue EJ, Roxburgh A, Yurchenko M (1998) Mater Res Bull 33:323
22. Saenger DU, Jung G (1998) J Sol–Gel Sci Technol 13:635
23. Zhang WH, Shi JL (2001) Chem Mater 13:648
24. Banerjee IA, Yu L, Matsui HJ (2005) Am Chem Soc 127:16002
25. Carl J, Barrelet YW (2003) J Am Chem Soc 125:11498
26. Cao CB, Zhu HS (2004) Mater Res Bull 39:1517
27. Richard K, Claudia L, Rajesh KM (2000) J Colloid Interface Sci 227:561
28. Pradhan N, Katz B, Efrima S (2003) J Phys Chem B 107:13843
29. Huang F, Zhang H, Banfield JF (2003) J Phys Chem B 107:10470
30. Vogel W (2000) Langmuir 16:2032
31. Nanda J, Sapra S, Sarma DD (2000) Chem Mater 12:1018
32. Li Y, Li X, Yang C, Li Y (2004) J Phys Chem B 108:16002
33. Ossenkamp GC, Kemmitt T, Johnston JH (2002) J Colloid Interface Sci 249:464
34. Winiarz JG, Zhang L, Park J, Prasad PN (2002) J Phys Chem B 106:967
35. Liu H, Zheng S, Nie K (2005) Macromolecules 38:5088
36. Jeffrey P, Krzystof M (2001) Chem Mater 13:3436
37. Park HM, Liang X, Mohanty AK, Misra M, Drzal LT (2004) Macromolecules 37:9076
38. Leu CM, Wu ZW, Wei KH (2002) Chem Mater 14:3016
39. Wang JW, Shen QD, Yang CZ, Zhang QM (2004) Macromolecules 37:2294
40. Takafuji M, Ide S, Ihara H, Xu Z (2004) Chem Mater 16:1977
41. Jordan R, West N, Ulman A, Chou YM, Nuyken O (2001) Macromolecules 34:1606
42. Liu T, Jia S, Kowalewski T, Matyjaszewski K, Belmont J (2006) Macromolecules 39:548
43. Fan X, Zhou Q, Xia C, Cristofoli W, Mays J, Advincula R (2002) Langmuir 18:4511
44. Li ZF, Swihart MT, Ruckenstein E (2004) Langmuir 20:1963
45. Hwang JI, Oh M, Kim L, Lee J, Ha CS (2005) Current Applied Physics 5:31
46. Bai C, Fang Y, Zhang Y, Chen B (2004) Langmuir 20:263
47. Pich A, Hain J, Lu Y, Boyko V, Prots Y, Adler HJ (2005) Macromolecules 38:6610
48. Lu CL, Cui ZC, WangY, Li Z, Yang B (2003) J Mater Chem 13:2189
49. Ni Y, Ge X, Zhang Z (2005) Mater Sci Eng 119:51
50. Chen S, Zhu J, Shen Y, Hu C, Chen L (2007) Langmuir 23:850
51. Lu CL, Cui ZC, Li Z, Yang B, Shen JC (2003) J Mater Chem 13:526
52. Yang Y, Huang JM, Liu SY, Shen JC (1997) J Mater Chem 7:131
53. Yu JH, Joo J, Park HM (2005) J Am Chem Soc 127:5662
54. Yang H, Zhao JZ, Song LZ (2003) Mater Lett 57:2287
55. Brus L (1986) J Phys Chem 90:2555
56. Wageh S, Ling ZS (2003) J Cryst Growth 255:332
57. Sapra S, Prakash A, Ghangrekar A, Periasamy N, Sarma DD (2005) J Phys Chem B 109:1663
58. Bhargava RN, Gallaghera D, Welkerb T (1994) J Lumin 60:275
59. Gu F, Li CZ, Wang SF (2006) Langmuir 22:1329
60. Aymonier C, Bortzmeyer D, Thomann R, Mulhaupt R (2003) Chem Mater 15:4874